EDGE ARTICLE

Check for updates

All publication charges for this article have been paid for by the Royal Society of Chemistry

Borohydride-containing coordination polymers: synthesis, air stability and dehydrogenation†

Kentaro Kadota,[a] Nghia Tuan Duong, [ID][b] Yusuke Nishiyama, [ID][bc] Easan Sivaniah, [ID][ad] Susumu Kitagawa[d] and Satoshi Horike [ID] *[defg]

Control of the reactivity of hydride (H^{−}) in crystal structures has been a challenge because of its strong electron-donating ability and reactivity with protic species. For metal borohydrides, the dehydrogenation activity and air stability are in a trade-off, and control of the reactivity of BH_4^- has been demanded. For this purpose, we synthesize a series of BH_4^--based coordination polymers/metal–organic frameworks. The reactivity of BH_4^- in the structures is regulated by coordination geometry and neighboring ligands, and one of the compounds [$Zn(BH_4)_2$(dipyridylpropane)] exhibits both high dehydrogenation reactivity (1.4 wt% at 179 °C) and high air stability (50 RH% at 25 °C, 7 days). Single crystal X-ray diffraction analysis reveals that $H^{\delta+}\cdots H^{\delta-}$ dihydrogen interactions and close packing of hydrophobic ligands are the key for the reactivity and stability. The dehydrogenation mechanism is investigated by temperature-programmed desorption, *in situ* synchrotron PXRD and solid-state NMR.

Controlling the reactivity of hydride-based ions in the solid state is important for hydrogen-related functions such as hydrogen (H_2) storage, heterogeneous hydrogenation catalysis and ion conduction.[1–3] Hydride-based ions include hydride (H^{−}) and molecular ions such as borohydride (BH_4^-) and alanate (AlH_4^-), and they exhibit a strong electron-donating ability.[4] The reactive character causes high sensitivity to moisture in the air, and it has been a challenge to design the dual properties of high reactivity of hydrides and air stability in the solid state. For example, the dehydrogenation reactivity and air stability are in a trade-off for BH_4^- in metal borohydrides (MBHs). Air-stable $NaBH_4$ releases H_2 above 500 °C, whereas $Al(BH_4)_3$ is pyrophoric in contact with moisture in the air, and it releases H_2 at 60 °C.[5,6] The properties of MBHs are affected by some parameters of metal ions – electronegativity and ionic radius.[7] A number of studies to tune the properties of MBHs were made (*e.g.*, mixed metal ion MBHs,[8–10] hybridization with organic polymers,[11] and nano-confinement in porous scaffolds[12,13]). The reactivity of BH_4^- in crystal structures depends on hydrogen–hydrogen interactions (*e.g.*, hydrogen bonding and dihydrogen bonding).[14,15] For the precise tuning of these interactions, we applied coordination polymers (CPs) and metal–organic frameworks (MOFs).[16–19] Tuning the coordination geometry and reactivity of metal ions or bridging ligands can afford the precise configuration of ions/molecules in CP architectures. CP structures are thought to be constructed with BH_4^-; however it has been unsuccessful because of the high reactivity of BH_4^-.

The attempts to incorporate reactive BH_4^- into CP structures readily lead to the reduction of metal ions or decomposition of organic ligands. There are many reports on polymeric crystal structures consisting of metal ions and bridging BH_4^-.[20] On the other hand, the extended BH_4^--based crystal structures constructed from metal ions and organic bridging ligands are limited: ([$Mg(BH_4)_2$(pyrazine)$_2$] and [$Th(OTer^{Mes})_2(BH_4)_2$(4,4′-bipyridyl)]) were the only examples reported in the Cambridge Crystallographic Data Centre (CCDC) database.[21,22] As shown in previous studies, neutral N-donor ligands are suitable to incorporate BH_4^- as a counter anion in CP structures. We then used commercially available $Mg(BH_4)_2$ and $Ca(BH_4)_2$ for CP synthesis using neutral N-donor ligands under Ar. The solution reaction using $Mg(BH_4)_2$ and 4,4′-bipyridyl in acetonitrile (MeCN) afforded a polymeric structure. $Ca(BH_4)_2$ with poor solubility in organic solvents is not suitable for solution reactions. A solvent-free mechanochemical reaction of $Ca(BH_4)_2$ and

[a]Department of Molecular Engineering, Graduate School of Engineering, Kyoto University, Katsura, Nishikyo-ku, Kyoto 615-8510, Japan

[b]RIKEN-JEOL Collaboration Center, Tsurumi, Yokohama, Kanagawa 230-0045, Japan

[c]JEOL RESONANCE Inc., Musashino, Akishima, Tokyo 196-8558, Japan

[d]Institute for Integrated Cell-Material Sciences, Institute for Advanced Study, Kyoto University, Yoshida, Sakyo-ku, Kyoto 606-8501, Japan. E-mail: horike@icems.kyoto-u.ac.jp

[e]AIST-Kyoto University Chemical Energy Materials Open Innovation Laboratory (ChEM-OIL), National Institute of Advanced Industrial Science and Technology (AIST), Yoshida-Honmachi, Sakyo-ku, Kyoto 606-8501, Japan

[f]Department of Synthetic Chemistry and Biological Chemistry, Graduate School of Engineering, Kyoto University, Katsura, Nishikyo-ku, Kyoto 615-8510, Japan

[g]Department of Materials Science and Engineering, School of Molecular Science and Engineering, Vidyasirimedhi Institute of Science and Technology, Rayong 21210, Thailand

pyrazine produced crystalline powder of CP. On the other hand, the synthetic attempts using other pyridyl-based ligands afforded amorphous powder or no solid product. This is because of a weak coordination interaction between hard Mg^{2+} or Ca^{2+} and soft N-donor ligands according to Hard and Soft Acids and Bases (HSAB) theory. The theory says that soft transition metal ions (e.g., Zn^{2+} and Mn^{2+}) form stable coordination bonds with N-donor ligands. $[PPh_4Zn(BH_4)_3]$ and $[Mn(BH_4)_2 \cdot 3THF] \cdot NaBH_4$ were therefore prepared as starting materials.[23] Bulky PPh_4^+ cations were incorporated to increase the solubility of the salt. Transition metal ion-based MBH precursors successfully form coordination bonds with pyridyl and imidazolate ligands, and 10 CP crystals were isolated as summarized in Fig. 1. In general, the structural analysis from a single crystal for MBH is difficult, and it is usually hard to determine the exact position of hydrogen atoms in BH_4^-.[24,25] In the present cases, high-quality single-crystal diffraction data enable us to locate the hydrogen atoms of BH_4^- in a Fourier map and refine freely without restraints. This is beneficial to understand the local structure of BH_4^- and the resulting properties.

As shown in Fig. 1, each product is classified according to the local coordination environments at the M^{2+} center (tetrahedral, trigonal bi-pyramidal and octahedral, where BH_4^- is assumed to occupy one site). As the coordination number of ligands increases, the M–B distance increases (tetrahedral: 2.339 Å, trigonal bi-pyramidal: 2.499 Å, and octahedral: 2.696 Å, Table S3†). Electron-donation from N-donor ligands to metal ions decreases the electronic interaction between M and BH_4^-.[21] The coordination mode of BH_4^- to metal ions was clearly determined, and most of them were bidentate. In addition, BH_4^- in the structures shows dihydrogen bonding with the hydrogen atoms of bridging ligands. A dihydrogen bond is an interaction between negatively charged hydrogen and positively charged hydrogen (e.g., $B–H^{\delta-}\cdots H^{\delta+}–C$, normally <2.4 Å), and affects the crystal packing and physical properties.[26] The number of dihydrogen bonds varies in the range of 0 to 3 as summarized in Table S3.† Four packing structures were observed, one-dimensional (1D) chain (1, 2, 3, 4), 1D ladder (5, 6, 7, 8), two-dimensional (2D) bilayer (9) and 2D sheet (10). The CPs with a higher coordination number of the ligands show higher structural dimensionality. 5, 6, 7 and 9 contain MeCN as guest molecules, and the permanent porosity of 5 and 6 was determined by N_2 and CO_2 adsorption (Fig. S27 and S28†).

Bulk powder samples were prepared under the same reaction conditions, and phase purity was confirmed by PXRD and infrared (IR) spectroscopy under Ar (Fig. S24 and S25†). The thermal properties were characterized by thermogravimetric analysis (TGA) under Ar (Fig. S26†). As various types of chemical environments of BH_4^- were observed in 1–10, the dependence of the air stability on the local structure was examined. Each powder sample (30 mg) was exposed to humidified air (relative humidity (RH) 50% at 25 °C, Fig. S29†), and time-course IR spectra and PXRD patterns were recorded to monitor BH_4^-. Reference MBHs, $NaBH_4$ and $Mg(BH_4)_2$ were also evaluated for comparison. After air exposure of $Mg(BH_4)_2$ for 3 hours, no peak is observed in the B–H region in the IR spectrum (Fig. 2A). The broad peak at 3500 cm^{-1} indicates the hydrolysis of BH_4^-. Although $NaBH_4$ is considered as an air-stable MBH, it showed deliquescence in 2 hours under the conditions and hydrolyzed to form $Na_2[B_4O_5(OH)_4] \cdot 3H_2O$
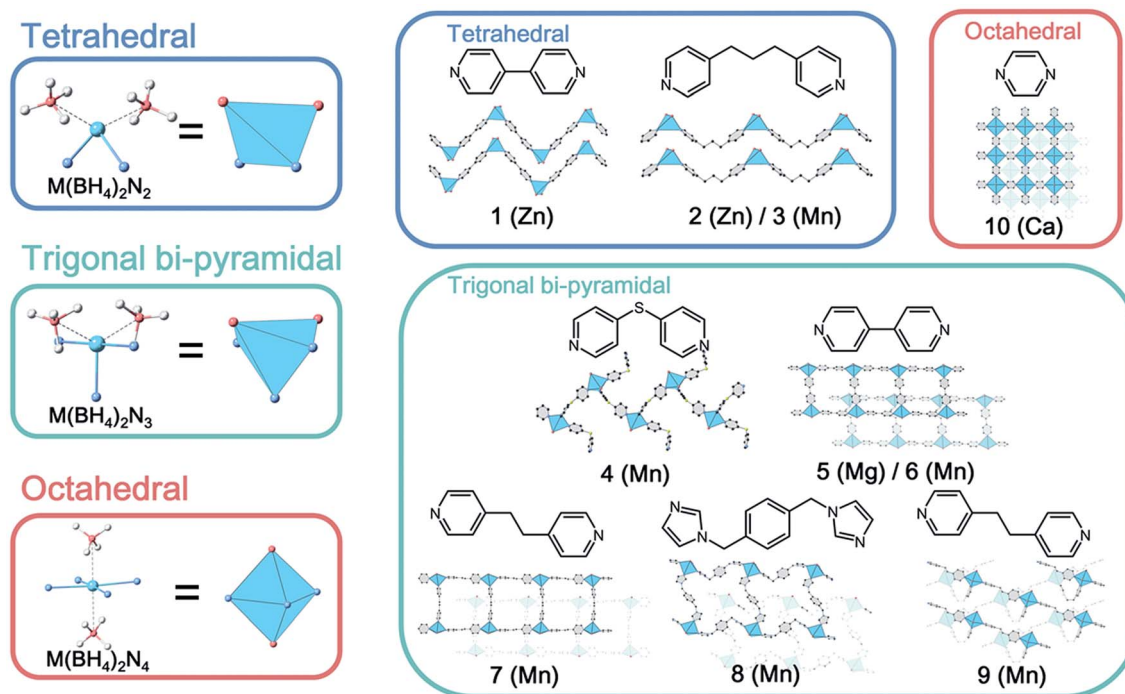

Fig. 1 Crystal structures of BH_4^--based CPs. Tetrahedral (1–3), trigonal bi-pyramidal (4–9) and octahedral (10) geometries, and constituent metal ions and ligands are represented, respectively.
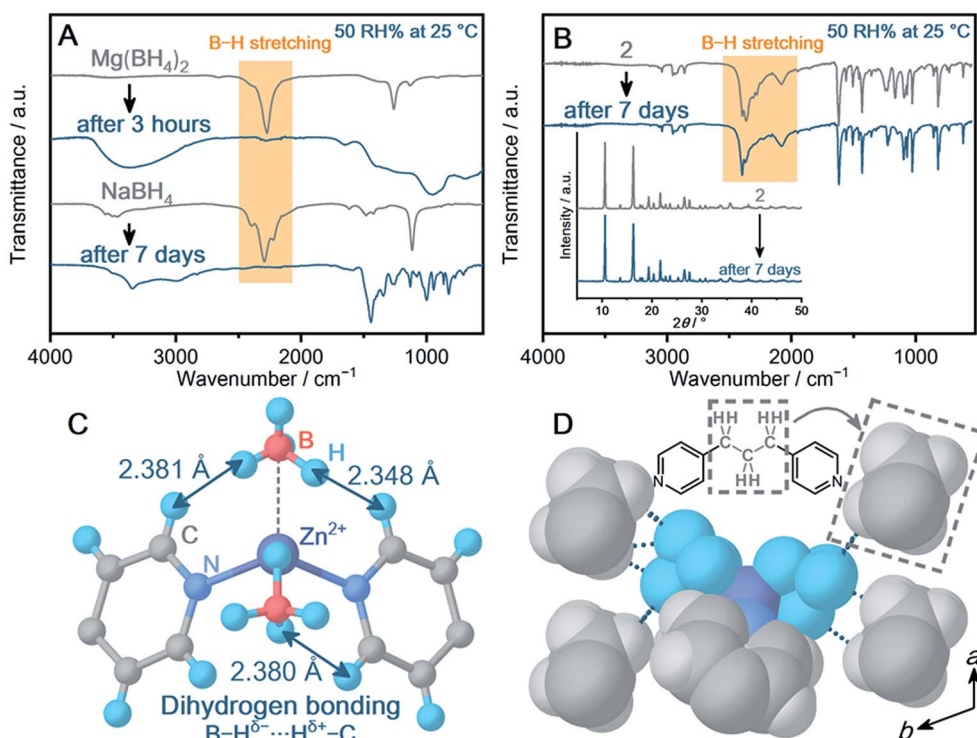
Fig. 2 (A) IR spectra of Mg(BH$_4$)$_2$ and NaBH$_4$ before and after the air exposure (50 RH% at 25 °C). (B) IR spectra and PXRD patterns (inset) of **2** before and after the air exposure (50 RH% at 25 °C) for 7 days. (C) Local coordination geometry of BH$_4^-$ in **2** from single-crystal X-ray diffraction analysis. The arrows represent the dihydrogen bonds between B–H$^{\delta-}$ and H$^{\delta+}$–C. (D) Packing structure of **2**. The short contacts between the hydrogen atoms of BH$_4^-$ and the aliphatic group of the surrounding dpp (–CH$_2$CH$_2$CH$_2$–) are displayed as a blue dotted line. The pyridyl rings of the neighbouring dpp are omitted for clarity.

after air exposure for 7 days (Fig. S30†). Humidified conditions are harsh enough to hydrolyze BH$_4^-$ in most of the MBHs.

Some crystalline powder samples changed to amorphous in a few minutes (**5**, Mg^{2+} and **10**, Ca^{2+}) or 1 day (**3–4**, **6–9**, Mn^{2+}). Notably, among the BH$_4^-$-CPs, Zn^{2+}-based CPs (**1** and **2**) exhibited high air stability. In particular, **2** exhibits IR spectra identical before and after air exposure for 7 days in Fig. 2B. In addition, **2** retains highly crystalline peaks in PXRD (Fig. 2B, inset). The results demonstrate improved air stability of **2**, and the mechanisms are discussed based on the crystal structure of **2**. Although many structural parameters affect the air stability, we classify the main contributions to the high air stability of **2** as the (i) metal–ligand coordination bond (ii) dihydrogen bonding and (iii) packing structure. **2** shows higher air stability than the isostructural Mn^{2+}-based **3**. In general, a metal–ligand bond is an essential parameter to determine the air stability of CPs.[27] The Zn–N bond in tetrahedral geometry is known to construct highly stable CPs.[28] Meanwhile, limited examples of CPs with Mn–N in tetrahedral geometry have been reported, and most of them are sensitive to air.[29,30] The tendency of air stability depending on metal ions is also suggested by a survey of the CCDC database.[31] Fig. 3C displays the dihydrogen bond between BH$_4^-$ and the neighboring dipyridylpropane (dpp) in the structure of **2**. In addition to the X-ray diffraction analysis, the geometry optimization on **2** utilizing DFT calculation suggests that dihydrogen bonds form as well (Fig. S46†). In general, dihydrogen bonding stabilizes a crystal structure by the electrostatic interaction between oppositely charged hydrogen atoms,[32,33] and the interaction lowers the electron donating ability of BH$_4^-$. The intermolecular interaction and packing structure are also essential for air stability, because they affect the diffusion of H$_2$O molecules in the structure. BH$_4^-$ is surrounded by the hydrophobic propyl group (2.545–3.010 Å) as shown in Fig. 2D, which avoids the attack of H$_2$O. In addition, the concentration of hydrophobic species around BH$_4^-$ of **2** was compared with that of other CPs showing different air stability. The number of carbon atoms away from the boron atoms of BH$_4^-$ within 5 Å was counted for **2**, **9** and **10** (Fig. S47†). **2** shows a higher concentration of carbon atoms than **9** and **10** (the total number of carbon atoms within 5 Å, **2**: 47, **9**: 39, **10**: 16), which also contributes to the high air stability of **2**.[34]

As **2** exhibited exceptionally high air stability, the dehydrogenation properties of **2** were characterized. The TGA profile under Ar exhibits a characteristic weight loss of 1.4 wt% at 170 °C with a second weight loss at 260 °C (Fig. S26†). The released chemical species at 170 °C were analyzed using temperature-programmed desorption (TPD) as shown in Fig. 3A. The release of H$_2$ ($mz = 2$) starts from 108 °C and peaks are observed at 179 and 203 °C in the TPD profile, corresponding to the weight loss (1.4 wt%) at 170 °C in TGA. The observed dehydrogenation temperature for **2** is higher than that of [NaZn(BH$_4$)$_3$] (103 °C),[8] which is due to the stabilization effect of BH$_4^-$ in **2**. In spite of
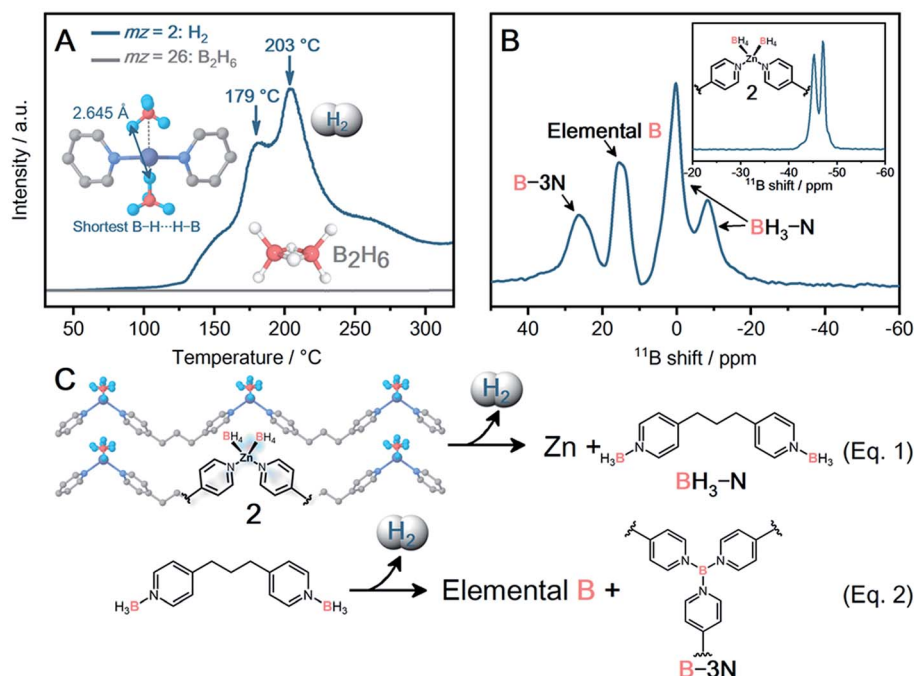
Fig. 3 (A) TPD profile of **2** under Ar. The release of H_2 (blue line) and B_2H_6 (gray line) was monitored. Inset: the shortest $B-H\cdots H-B$ distance is displayed. (B) Solid-state ^{11}B MAS NMR spectra of **2** before (inset) and after dehydrogenation. (C) Schematic illustration of the proposed dehydrogenation mechanism of **2**.

the higher air stability of **2** than $NaBH_4$, **2** exhibits a lower dehydrogenation temperature than $NaBH_4$ (170 vs. 505 °C). Note that dpp ligands decrease the amount of H_2 release per weight, and the 1.4 wt% of H_2 is smaller than that of the MBHs. The close contact of each BH_4^- enables dehydrogenation at a lower temperature. The inset of Fig. 3A displays the closest distance between $B-H\cdots H-B$ (2.645 Å), which is comparable to that of Zn^{2+}-based MBHs ([$LiZn_2(BH_4)_5$]: 2.482 Å; [$NaZn(BH_4)_3$]: 2.291 Å).[8] Tetrahedral geometry in **2** is suitable to arrange BH_4^- in close proximity. The variable temperature synchrotron PXRD experiments indicate the structural expansion of **2** upon heating (25–226 °C, Fig. S38 and S39†). **2** does not exhibit an amorphous phase before dehydrogenation at 179 °C, and metallic Zn peaks are observed above 180 °C. The dehydrogenation of two BH_4^- produces one molecule of H_2 and subsequently reduces Zn^{2+} to metallic Zn.

The environment of BH_4^- after the dehydrogenation was characterized by solid-state ^{11}B magic angle spinning (MAS) nuclear magnetic resonance (NMR). The ^{11}B NMR spectrum of pristine **2** shows two peaks at −45 and −47 ppm, and both peaks correspond to crystallographically independent BH_4^- (Fig. 3B, inset).[8] The dehydrogenized **2** displays ^{11}B peaks at −8, 0, 15, and 30 ppm in Fig. 3B, and was further characterized by using the 2D multi-quantum (MQ) MAS NMR spectrum (Fig. S42†). To identify the resultant boron species, a 2D ^1H-{^{11}B} through-bond heteronuclear multiple quantum coherence (HMQC) experiment was performed (Fig. S43†). The ^{11}B peaks observed at −8 and 0 ppm correlate with the proton at 2 ppm, indicative of a B–H bond. These boron species are assigned to the [$(BH_3)_2dpp$] complexes.[35] Meanwhile, the remaining two ^{11}B

peaks (15, 30 ppm) do not exhibit a clear correlation, indicating no direct bond between these boron species and hydrogen atoms. The ^{11}B peak at 15 ppm corresponds to elemental boron and matches well with the simulated one (Fig. S44†), while the ^{11}B peak at 30 ppm corresponds to B-3N species (e.g., [$B(dpp)_x$]).[36–38] The 2D $^1H/^{13}C$ heteronuclear correlation spectrum clearly exhibits the ^1H and ^{13}C peaks corresponding to the aromatic ring and aliphatic chain of dpp, indicating that dpp does not decompose during dehydrogenation (Fig. S45†).

The first peak of H_2 release at 179 °C in TPD corresponds to the dehydrogenation of BH_4^- (eqn (1)). The release of toxic B_2H_6 is suppressed by the complexation with the N-donor dpp ligand to form [$(BH_3)_2dpp$] as revealed by solid-state NMR and IR spectra (Fig. S40†). The second peak of H_2 release at 203 °C in TPD corresponds to the further dehydrogenation of [$(BH_3)_2dpp$]. Solid-state NMR suggests that [$(BH_3)_2dpp$] partly forms elemental boron and B-3N species such as [$B(dpp)_x$] through the dehydrogenation (eqn (2)). **2** arranged BH_4^- and nitrogen atoms of dpp close to each other in a 1 : 1 ratio ($B\cdots N$ distance: 3.450 and 3.462 Å, Fig. S35†). **2** maintains the crystal structure before dehydrogenation at 179 °C as observed by in situ PXRD. The results indicate that the pre-organized environment of BH_4^- in **2** is preserved before the dehydrogenation, leading to the release of pure H_2 without B_2H_6.

Conclusions

By considering suitable combinations of metal ions and N-donor ligands, we have constructed 10 coordination polymer crystals involving reactive BH_4^- with various coordination
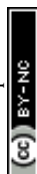
geometries. In particular, [Zn(BH₄)₂(dipyridylpropane)] (2) demonstrated both high dehydrogenation reactivity and high air stability. The crystal structure of **2** was intact under humidified conditions (50 RH% at 25 °C, 7 days) which indicates exceptionally high air stability as compared with conventional MBHs. This is due to the strong metal–ligand bond, the electrostatic stabilization by dihydrogen bonding, and close packing of the hydrophobic group with BH_4^-. In spite of the stabilization of BH_4^-, the dehydrogenation reactivity was maintained (pure H_2, 1.4 wt%, 179 °C). Tetrahedral geometry in **2** arranged two BH_4^- closely, which accelerated the dehydrogenation. We demonstrated that crystal engineering of coordination polymers and metal–organic frameworks expands the library of hydride-based crystal structures and their properties.

Conflicts of interest

There are no conflicts to declare.

Acknowledgements

References

1 T. He, P. Pachfule, H. Wu, Q. Xu and P. Chen, *Nat. Rev. Mater.*, 2016, **1**, 16059.

2 G. Kobayashi, Y. Hinuma, S. Matsuoka, A. Watanabe, M. Iqbal, M. Hirayama, M. Yonemura, T. Kamiyama, I. Tanaka and R. Kanno, *Science*, 2016, **351**, 1314–1317.

3 M. Kitano, Y. Inoue, Y. Yamazaki, F. Hayashi, S. Kanbara, S. Matsuishi, T. Yokoyama, S.-W. Kim, M. Hara and H. Hosono, *Nat. Chem.*, 2012, **4**, 934–940.

4 Z. M. Heiden and A. P. Lathem, *Organometallics*, 2015, **34**, 1818–1827.

5 J. F. Mao and D. H. Gregory, *Energies*, 2015, **8**, 430–453.

6 Y. Nakamori, H. W. Li, K. Kikuchi, M. Aoki, K. Miwa, S. Towata and S. Orimo, *J. Alloys Compd.*, 2007, **446–447**, 296–300.

7 Y. Nakamori, K. Miwa, A. Ninomiya, H. Li, N. Ohba, S. Towata, A. Züttel and S. Orimo, *Phys. Rev. B: Condens. Matter Mater. Phys.*, 2006, **74**, 045126.

8 D. Ravnsbæk, Y. Filinchuk, Y. Cerenius, H. J. Jakobsen, F. Besenbacher, J. Skibsted and T. R. Jensen, *Angew. Chem., Int. Ed.*, 2009, **121**, 6787–6791.

9 T. Jaroń, P. A. Orłowski, W. Wegner, K. J. Fijałkowski, P. J. Leszczyński and W. Grochala, *Angew. Chem., Int. Ed.*, 2015, **54**, 1236–1239.

10 R. Černý, P. Schouwink, Y. Sadikin, K. Stare, L. u. Smrčok, B. Richter and T. R. Jensen, *Inorg. Chem.*, 2013, **52**, 9941–9947.

11 J. Huang, Y. Yan, L. Ouyang, H. Wang, J. Liu and M. Zhu, *Dalton Trans.*, 2014, **43**, 410–413.

12 E. Callini, P. Á. Szilágyi, M. Paskevicius, N. P. Stadie, J. Réhault, C. E. Buckley, A. Borgschulte and A. Züttel, *Chem. Sci.*, 2016, **7**, 666–672.

13 P. N. Suwarno, A. Nale, T. M. Eggenhuisen, M. Oschatz, J. P. Embs, A. Remhof and P. E. de Jongh, *J. Phys. Chem. C*, 2017, **121**, 4197–4205.

14 R. Custelcean and J. E. Jackson, *Chem. Rev.*, 2001, **101**, 1963–1980.

15 D. J. Wolstenholme, J. L. Dobson and G. S. McGrady, *Dalton Trans.*, 2015, **44**, 9718–9731.

16 O. M. Yaghi, M. O'Keeffe, N. W. Ockwig, H. K. Chae, M. Eddaoudi and J. Kim, *Nature*, 2003, **423**, 705–714.

17 S. Kitagawa, R. Kitaura and S. Noro, *Angew. Chem., Int. Ed.*, 2004, **43**, 2334–2375.

18 G. Ferey, *Chem. Soc. Rev.*, 2008, **37**, 191–214.

19 S. R. Batten, N. R. Champness, X.-M. Chen, J. Garcia-Martinez, S. Kitagawa, L. Öhrström, M. O'Keeffe, M. Paik Suh and J. Reedijk, *Pure Appl. Chem.*, 2013, **85**, 1715–1724.

20 V. D. Makhaev, *Russ. Chem. Rev.*, 2000, **69**, 727–746.

21 M. J. Ingleson, J. P. Barrio, J. Bacsa, A. Steiner, G. R. Darling, J. T. A. Jones, Y. Z. Khimyak and M. J. Rosseinsky, *Angew. Chem., Int. Ed.*, 2009, **48**, 2012–2016.

22 J. McKinven, G. S. Nichol and P. L. Arnold, *Dalton Trans.*, 2014, **43**, 17416–17421.

23 V. D. Makhaev, A. P. Borisov, T. P. Gnilomedova, É. B. Lobkovskii and A. N. Chekhlov, *Bull. Acad. Sci. USSR, Div. Chem. Sci.*, 1987, **36**, 1582–1586.

24 Y. Filinchuk, R. Černý and H. Hagemann, *Chem. Mater.*, 2009, **21**, 925–933.

25 Y. Filinchuk, D. Chernyshov and R. Cerny, *J. Phys. Chem. C*, 2008, **112**, 10579–10584.

26 N. V. Belkova, L. M. Epstein, O. A. Filippov and E. S. Shubina, *Chem. Rev.*, 2016, **116**, 8545–8587.

27 N. C. Burtch, H. Jasuja and K. S. Walton, *Chem. Rev.*, 2014, **114**, 10575–10612.

28 K. S. Park, Z. Ni, A. P. Cote, J. Y. Choi, R. Huang, F. J. Uribe-Romo, H. K. Chae, M. O'Keeffe and O. M. Yaghi, *Proc. Natl. Acad. Sci. U. S. A.*, 2006, **103**, 10186–10191.

29 K. Kadota, E. Sivaniah, S. Bureekaew, S. Kitagawa and S. Horike, *Inorg. Chem.*, 2017, **56**, 8744–8747.

30 K. Müller-Buschbaum and F. Schonfeld, *CSD Communication*, 2014.

31 In CCDC database, the reported examples of [Zn(X)₂(pyridyl)₂] are greater than twice of the hydrated geometry, [Zn(X)₂(pyridyl)₂(H₂O)₂] (1306 *vs.* 814 hits). By contrast, Mn^{2+} prefers the hydrated structure (unhydrated: 28 hits, hydrated: 375 hits).

32 J. Fanfrlik, M. Lepsik, D. Horinek, Z. Havlas and P. Hobza, *ChemPhysChem*, 2006, **7**, 1100–1105.

33 I. V. Glukhov, K. A. Lyssenko, A. A. Korlyukov and M. Y. Antipin, *Russ. Chem. Bull.*, 2005, **54**, 547–559.

34 X. Zhao, H. Yang, E. T. Nguyen, J. Padilla, X. Chen, P. Feng and X. Bu, *J. Am. Chem. Soc.*, 2018, **140**, 13566–13569.

35 P. Veeraraghavan Ramachandran, A. S. Kulkarni, Y. Zhao and J. Mei, *Chem. Commun.*, 2016, **52**, 11885–11888.

36 G. Xia, Q. Gu, Y. Guo and X. Yu, *J. Mater. Chem.*, 2012, **22**, 7300–7307.

37 C. L. Turner, R. E. Taylor and R. B. Kaner, *J. Phys. Chem. C*, 2015, **119**, 13807–13813.

38 P. M. I. Irene, A. C. Armando and C. Rosalinda, *Magn. Reson. Chem.*, 1993, **31**, 189–193.